Chinese Chemical Letters 37 (2026) 112199

Contents lists available at ScienceDirect

Chinese Chemical Letters

journal homepage: www.elsevier.com/locate/cclet

Size-controlled synthesis of N-doped [10]CPPs and investigation on the variations of their binding affinities with fullerene

Tianlu Wu[a,1], Jiaojiao Yang[a,1], Yaru Liu[a], Chen Wang[a], Jiwen Zhang[a], Ren-Hui Zheng[c], Huan Yu[a,*], Rui Liu[b,*], Dapeng Lu[a,*]

[a] Inflammation and Immune Mediated Diseases Laboratory of Anhui Province, The Key Laboratory of Antiinflammatory and Immune Medicine, Ministry of Education, School of Pharmacy, Anhui Medical University, Hefei 230032, China
[b] School of Basic Medical Sciences, Anhui Medical University, Hefei 230032, China
[c] Beijing National Laboratory for Molecular Sciences, State Key Laboratory for Structural Chemistry of Unstable and Stable Species, Institute of Chemistry, Chinese Academy of Sciences, Beijing 100190, China

ARTICLE INFO

Article history:
Received 11 August 2025
Revised 16 November 2025
Accepted 28 November 2025
Available online 29 November 2025

Keywords:
Cycloparaphenylenes
Size-controlled synthesis
Host-guest chemistry
Nitrogen-doping
Fullerene

ABSTRACT

Cycloparaphenylenes (CPPs) and related carbon nanohoops have garnered significant research interest owing to their unique optoelectronic properties, charge transport characteristics, and host-guest chemistry. Nevertheless, the development of heteroatom-doped carbon nanorings, particularly nitrogen-doped (N-doped) systems, remains limited, and systematic investigations of their host-guest interactions are still scarce. In this work, we present the synthesis of a series of size-controlled aza[10]CPP derivatives designed as optimal hosts for fullerene C_{60} encapsulation. The acid-responsive optical properties of these N-doped nanorings were thoroughly examined through absorption and fluorescence spectroscopy. Furthermore, we experimentally evaluated and theoretically analyzed the variations in their binding affinities toward C_{60}, elucidating key structural factors that govern supramolecular complexation, including π-π stacking interactions, geometric adaptability, and charge distribution. These findings would provide new insights for advancing strained nanohoop systems in supramolecular chemistry and organic electronic applications.

© 2026 Published by Elsevier B.V. on behalf of Chinese Chemical Society and Institute of Materia Medica, Chinese Academy of Medical Sciences.

Cycloparaphenylenes (CPPs) represent the simplest structural fragments of armchair carbon nanotubes (CNTs), characterized by unique radially oriented cyclic π-conjugation systems that endow them with remarkable optoelectronic properties, self-assembly behavior, and charge transport characteristics [1–5]. Although extensive efforts have been made toward the synthesis of CPPs, the first successful preparations were not accomplished until 2008–2009, when three independent research groups reported distinct synthetic strategies [6]. During the past decade, the structural diversification of CPPs was extensively expanded, such as CPPs with varied diameters [6,7], polyaromatic hydrocarbon (PAH) incorporated macrocycles [8–15], donor- and/or acceptor-functionalized derivatives [16–19], and mechanically interlocked carbon nanoring systems [20,21]. These developments facilitated the exploration of CPPs and their derivatives for various applications, such as solution- and solid-state fluorophores [22–25], electronic devices [26,27], and components for the construction of host-guest nanomaterials [28–36].

In contrast to CNTs, CPPs possess atomically precise structures, enabling systematic modulation of their properties through controlled bottom-up synthesis and structural modifications, such as selective incorporation of heteroatoms into carbon nanoring skeletons, which is appealing to scientists [37–48]. The first nitrogen-doped (N-doped) CPP (cyclo[14]paraphenylene[4]2,5-pyridylidene) was reported in 2012 by Itami and co-workers [49]. The embedded bipyridine moieties enabled both protonation to induce bathochromic shift in photophysical properties and coordination as a palladium ligand. Later, Jasti's group developed a series of aza[8]CPPs (Fig. 1a), revealing that N-doping only slightly modifies the nanorings' properties. However, alkylation of these azananohoops would afford donor-acceptor architectures, leading to significant bathochromically shifted emission but with reduced intensity and less negative cathodic peak potentials [50]. Furthermore, a 2,2′-bipyridine-embedded [8]CPP was developed by the same group to construct a Pd(II)-nanohoop dimer and a bis(bipyridyl)ruthenium(II)-functionalized nanohoop, showing unique solid-state and photophysical properties [51]. They

* Corresponding authors.
E-mail addresses: hyu@iim.ac.cn (H. Yu), liurui@ahmu.edu.cn (R. Liu), ludapeng@ahmu.edu.cn (D. Lu).
[1] These authors contributed equally to this work.

https://doi.org/10.1016/j.cclet.2025.112199
1001-8417/© 2026 Published by Elsevier B.V. on behalf of Chinese Chemical Society and Institute of Materia Medica, Chinese Academy of Medical Sciences.

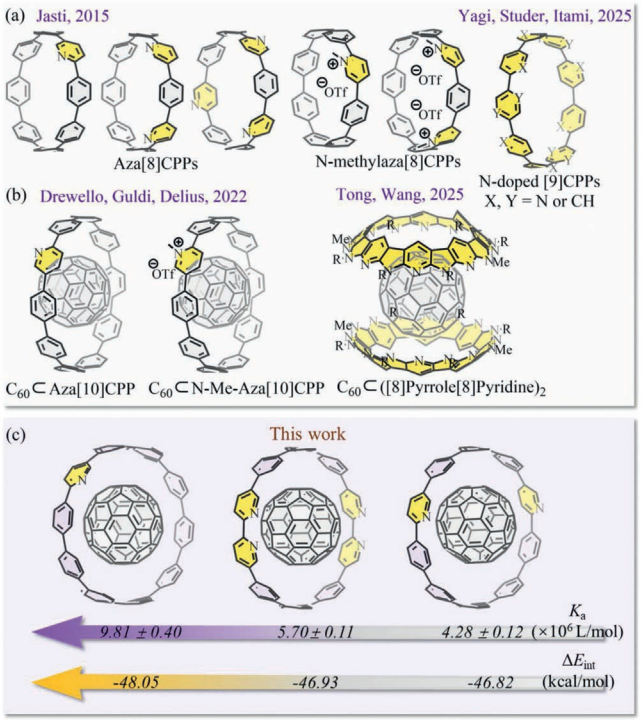


Fig. 1. Previously reported examples of (a) N-doped nanohoops and (b) host-guest systems between N-doped nanohoops and fullerenes. (c) Present work of N-doped CPPs with controlled size and variation of their binding affinities toward fullerene.

also exploited the coordinative ability of pyridyl nitrogen in an active-template synthesis of N-doped catenanes [21]. Recently, Quinton, Poriel and co-workers demonstrated electronic tuning of nanohoops by appending electron-accepting pyridine/pyrimidine units at the rim of [4]cyclo2,7-carbazole [52]. Yagi, Studer, Itami and co-workers synthesized highly N-doped nanorings, including one consisting solely of *N*-heterocycle, and uncovered the impact of both the amount and positioning of N-doping on the nanorings' properties (Fig. 1a) [53].

Additionally, the host-guest complexation was also achieved between the heteroatom-incorporated nanohoops and fullerenes [54]. For example, Zhu, Cong and co-workers constructed a fully conjugated thiophene-containing bis-macrocycles, the rigid yet guest-adaptive cavities of which enabled the formation of peanut-like 1:2 host-guest complexes with fullerenes [55]. Drewello, Guldi, Delius and co-workers synthesized aza[10]CPP and its *N*-methylated derivative, and unveiled their C_{60} binding affinities in solution and the gas phase (Fig. 1b) [56]. Very recently, Tong, Wang and co-workers synthesized a cone-shaped all-azine carbon nanobelt, which can serve as an outstanding host to form stable 2:1 encapsulation complexes with fullerenes (Fig. 1b) [57]. Comparison of selected properties between these reported N-doped nanohoops and aza[10]CPP derivatives in this work are summarized in Table S1 (Supporting information).

Despite these achievements, the systematic study of the host-guest behavior between heteroatom-containing nanohoops and fullerenes remains underexplored [58]. The investigation on this issue is driven not merely by the novelty of their structures but also by the need to provide a feasible strategy to introduce handles that would enable the regulation of their properties, as well as to elucidate the key structural factors that govern supramolecular complexation. In this work, we described the synthesis of a series of azaCPPs with controlled size as [10]CPP which would make them ideal hosts to complex with fullerene C_{60} (Fig. 1c). The impact of N-doping with different degrees on their optical properties and binding affinities was investigated both experimentally and theoretically, which would provide new insight for further applications of strained nanohoops in supramolecular chemistry and organic electronics.

Our investigations began by developing a synthetic methodology that would allow single, or isolated multi-pyridyl, or 2,2′-bipyridyl to be embedded in CPPs in a size-selective manner. Previous work has shown that CPPs and related derivatives can be accessed by the reductive aromatization of macrocycles containing cyclohexadienes as "masked" aromatic rings [59]. These relatively unstrained macrocycles can be prepared in a variety of sizes *via* aryl-aryl coupling reactions, which would also be effective in this work. For the construction of 2,2′-bipyridyl-embedded CPPs, however, the most general synthetic strategy would be one that forms the pyridine-pyridine linkage in the macrocyclization step due to the instability of 2-pyridylboranes. Therefore, we targeted nickel-mediated Yamamoto coupling of pyridyl halides as the key cyclization step. In order to leverage previous methods relying on the orthogonal reactivity of aryl halides, the use of pyridyl chlorides over bromides allows for orthogonal lithium-halogen exchange and Suzuki-Miyaura coupling for general access to the 2,2′-bipyridyl embedded nanohoops. Guided by these thoughts as well as previous works, we prepared single pyridyl-embedded precursor **6** [50], C-shaped synthons **7** [60] and **8** [60] by the reported method. We also prepared the key precursor **5b** with terminal pyridyl chloride units *via* addition of aryllithium from **3b** to ketone **4** in good yield (see Supporting information for the full synthetic route). The macrocycle intermediates **9a** and **9b** can be readily accessed by Suzuki-Miyaura cross-coupling of bromide **7** and boronic ester **6**, or pyridyl chloride **5b** and boronic ester **8** under palladium catalysis conditions. The 2,2′-bipyridyl embedded macrocycle intermediate **9c** was able to be accessed under nickel homocoupling conditions (Fig. 2). The final reductive aromatization step using the mild H_2SnCl_4 strategy [61] afforded the desired single, or isolated double pyridyl, or double 2,2′-bipyridyl embedded CPPs in 3 % yield for **1a**, 5 % for **1b**, and 3 % for **1c**, respectively, over two steps.

The structures of these pyridine-embedded CPPs were first confirmed by high-resolution MALDI-TOF MS (Figs. 3a, c and e). The main peak was observed at *m/z* 761.3438 (calcd. for $C_{59}H_{39}N$ $[M]^+$: 761.3083) for **1a**, 762.2840 (calcd. for $C_{58}H_{38}N_2$ $[M]^+$: 762.3035) for **1b**, and 764.2946 (calcd. for $C_{56}H_{36}N_4$ $[M]^+$: 764.2940) for **1c**, respectively. The isotopic distribution patterns were in good agreement with the simulated values. The ^1H NMR spectrum of **1a** with a single nitrogen atom doped shows dissymmetric signals, which differ from that of its parent structure of [10]CPP. The characteristic peaks at around 8.8 ppm at a lower field can be attributed to proton A in the pyridyl moiety due to electron-withdrawing effect of the nitrogen atom. Another two pyridyl protons B and C can also be assigned (Fig. 3b). Although the double pyridine-embedded CPP **1b** which has symmetric distribution of nitrogen atoms exhibits similar signal patterns as **1a** (Fig. 3d), the double 2,2′-bipyridyl embedded **1c** shows simplified signal patterns due to the highly symmetric structure, resulting in a decrease in the number of hydrogen peaks (Fig. 3f). These results suggested the successful synthesis of the targeted molecules.

Iso-chemical shielding surface (ICSS) analysis was also performed to reveal the influence of N-doping on magnetic shielding and deshielding effect (Fig. 3g). The pink isosurface represents the magnetic shielding regions filling the interior and outward of the carbon nanorings. The enhanced magnetic shielding effect in the cavity of carbon nanorings indicates that the aryl units arrange to form a tubular structure. The yellow isosurface represents the magnetic deshielding regions which are located around the rims of the aryl units. N-doping results in merging of adjacent deshielding regions instead of an alternating pattern for phenyl units (see Fig. S5 in Supporting information for details). This will enhance the

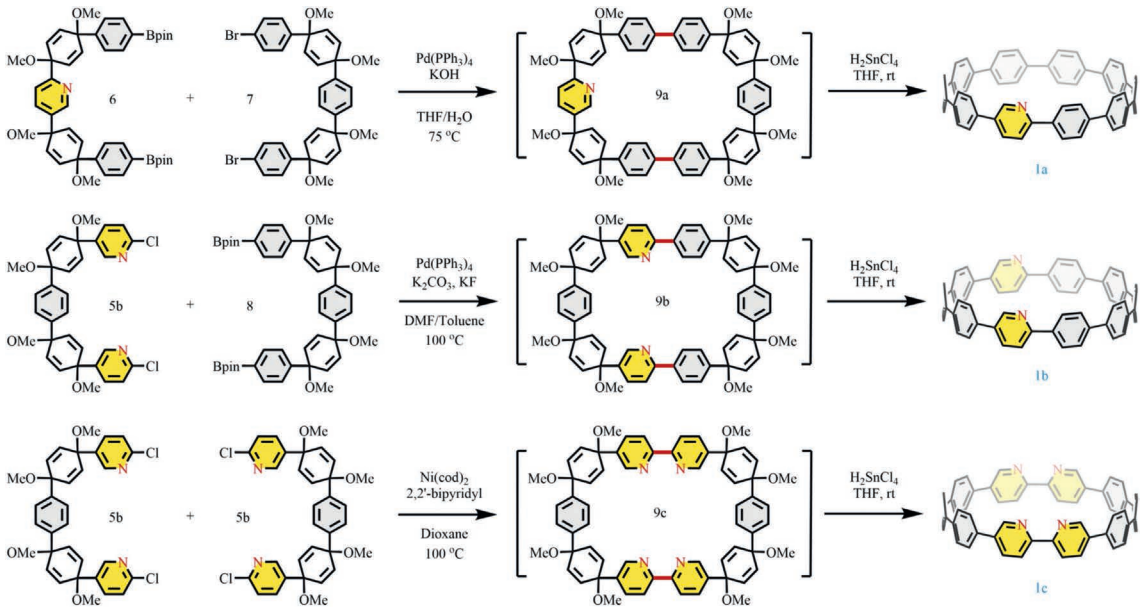


Fig. 2. Synthesis procedures for aza[10]CPP (**1a**), diaza[10]CPP (**1b**), and tetraaza[10]CPP (**1c**).

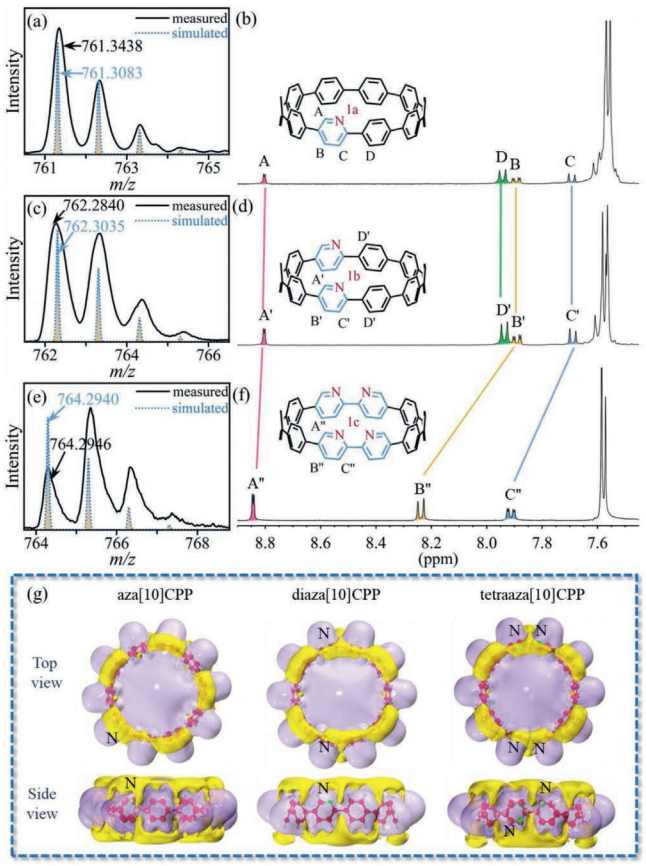


Fig. 3. HR-MS (MALDI-TOF MS) and simulated data for (a) **1a**, (c) **1b**, and (e) **1c**. Partial ^{1}H NMR spectra ($CDCl_3$, 400 MHz) of (b) **1a**, (d) **1b**, and (f) **1c** and assignment of pyridyl protons. (g) Isosurface maps (isovalue = 0.55 ppm) of ICSS for **1a**, **1b**, and **1c**. Pink and yellow isosurfaces correspond to shielding and deshielding regions, respectively.

deshielding effect which is accordance with the trends of proton signals in ^{1}H NMR.

The ground-state geometries were optimized at the B3LYP-D3/6–31G(d) level. Aza[10]CPP (**1a**), diaza[10]CPP (**1b**), and tetraaza[10]CPP (**1c**) exhibit C_1, C_s and C_2 point group symmetry, respectively. Due to the insertion of nitrogen atoms, the shapes of the molecules are no longer regular circles. Aza[10]CPP (**1a**) is closer to an ideal cylindrical shape, whereas diaza[10]CPP (**1b**) and tetraaza[10]CPP (**1c**) are relatively more deviated from the ideal cylinder (Figs. S6 and S7 in Supporting information). Furthermore, multiple insertions of nitrogen atoms would also reduce the torsion angles between the pyridyl and adjacent phenyl unit (4° and 2° for diaza[10]CPP (**1b**) and tetraaza[10]CPP (**1c**), respectively) (Table S3 in Supporting information). Although **1a-1c** show only slight differences in molecular diameter and dihedral angles, these subtle structural variations exert measurable effects on intermolecular interactions, particularly π-π stacking, in the supramolecular systems (which are discussed in the Host-guest Properties). Strain energies were estimated to be 56.4, 55.5, and 55.6 kcal/mol for aza[10]CPP (**1a**), diaza[10]CPP (**1b**), and tetraaza[10]CPP (**1c**), respectively using hypothetical homodesmotic reaction method (Fig. S8 and Table S4 in Supporting information) [62]. StrainViz analysis reveals that the strain is predominantly distributed around the single bonds connecting the benzene rings (Fig. S9 in Supporting information) [63].

All [*n*]CPPs have a common maximum absorbance at around 340 nm and almost no absorbance in the visible light. To gain a deeper understanding of the effect of N-doping on the optical properties of the azananorings, we investigated the UV–visible absorption spectra of aza[10]CPP **1a**-**1c** combined with theoretical calculations by time-dependent density functional theory (TDDFT) [64]. The first excited state (S_1) is still transition forbidden for all three molecules. The main absorption peak (λ_{max}) was observed at 343 nm ($\varepsilon = 1.3 \times 10^5$ cm^{-1} M^{-1}) for **1a**, 345 nm ($\varepsilon = 1.4 \times 10^5$ cm^{-1} M^{-1}) for **1b**, and 357 nm ($\varepsilon = 6.0 \times 10^4$ cm^{-1} M^{-1}) for **1c**, respectively, which is mainly contributed by the excitation from ground state (S_0) to the second and third excited states (S_2 and S_3) (Figs. 4a-c). Theoretical calculations reveal that the main excitations involve electron transitions between multiple molecular orbitals with corresponding weighting coefficients (left panels in Figs. 4d-f, and Tables S5-S7 in Supporting information). Consequently, it is difficult to examine the characteristics of the transitions by simply using single frontier orbital pairs. To better understand the intramolecular charge transfer, hole-electron analysis was conducted using Multiwfn [65,66]. The analysis shows that

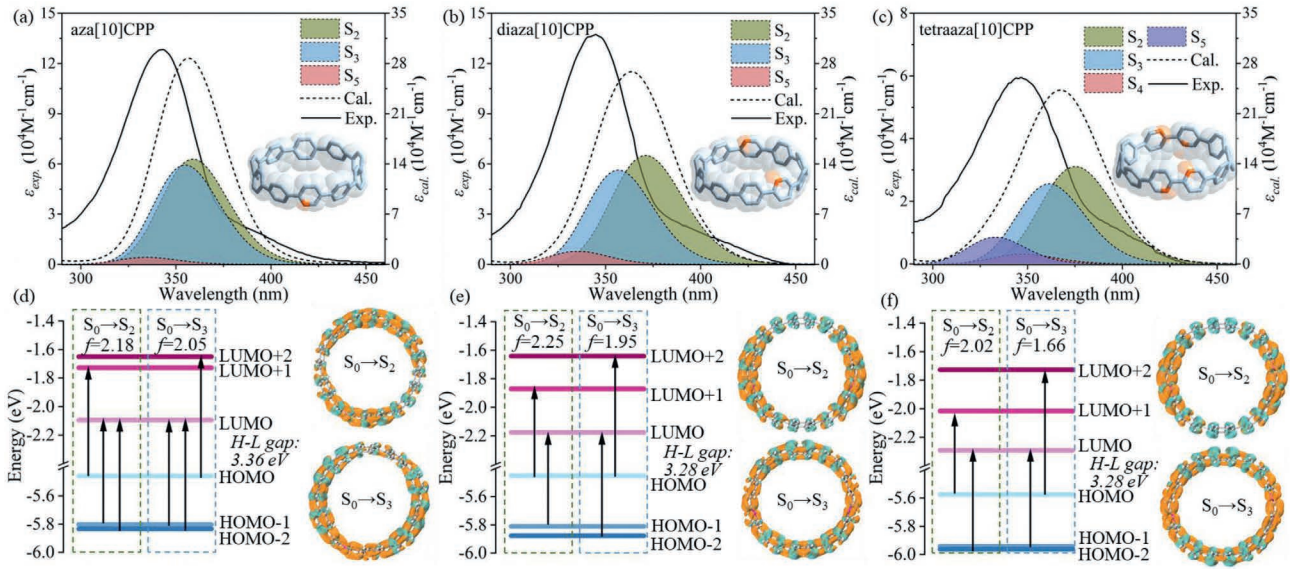


Fig. 4. Experimental (solid lines) and calculated (dashed lines) UV–vis absorptions of (a) **1a**, (b) **1b**, and (c) **1c** with separated contributions from different excited states. The experimental spectra were measured in chloroform with a concentration of 2.0×10^{-6} mol/L at room temperature. The calculated absorption profiles were obtained by an effective Gaussian full width half maximum (FWHM) of 0.4 eV. Insets: optimized structures of **1a-1c**. The energy diagrams (left panels) and hole-electron distributions (right panels) of main excited states ($f > 1$) for (d) **1a**, (e) **1b**, and (f) **1c**. The f value represents the oscillator strength. In the hole-electron distributions, blue and orange regions (isovalue = 0.0006) represent the hole and the electron distributions, respectively.

electrons move from "holes" (blue regions) to "electrons" (orange regions) upon excitation. All three molecules exhibit a global excitation feature in their main transitions, with electron transfer occurring across nearly the entire molecular structure (Figs. 4d-f, right panels). The fluorescence (λ_{em}) of **1a**-**1c** slightly shifted to 475, 478, and 483 nm, respectively relative to the emission wavelength of [10]CPP (466 nm) (Fig. S1 in Supporting information). The fluorescence quantum yields (Φ_F) are determined to be 52 %, 43 % and 61 % for **1a**-**1c**, respectively (using quinine sulfate in 0.1 mol/L H_2SO_4 as the standard with $\Phi_F = 54$ %).

One of the unique features of N-doped CPPs is their protonated states. Here we investigated the acid responses of these molecules through the steady-state UV-visible absorption and emission spectra. Upon continuous addition of trifluoroacetic acid (TFA), we first noted that the intensity of the main absorption peak demonstrates an incremental decrease for all the azananohoops (Figs. 5a, d and g). For **1b** and **1c**, however, two shoulder absorptions arise at shorter (331 nm for **1b**, and 324 nm for **1c**) and longer wavelengths (383 nm for **1b**, and 392 nm for **1c**) as TFA concentration increases, which are different from those of previously reported aza[*n*]CPPs [49,67]. On the other hand, the emission peak shows obvious red-shifts with $\Delta\lambda_{em}$ approximately 60 nm upon the addition of TFA along with decreased intensity, suggesting that the protonated product is obviously less emissive than the unprotonated species (Figs. 5b, e and h). Note that the emission intensity of **1b** experienced a dramatic enhancement at low TFA concentrations, and the luminescence of **1a** and **1b** has not been completely quenched even at high TFA concentrations. For **1c**, however, the luminescence can be nearly completely quenched along with the addition of acid. The chromaticity changes can be clearly viewed in the CIE coordinate diagrams (Figs. 5c, f and i), with photoluminescence images of **1a-1c** at varying TFA concentrations shown in the insets ($\lambda_{exc} = 365$ nm). At last, the protonation reaction was observed to be reversible by the recovery of fluorescence intensity upon the addition of triethylamine. To clarify protonation mechanisms, ^{1}H NMR under acidic conditions and DFT-based calculations for protonation constants (K^H) were conducted. Upon the addition of TFA, remarkable shifts of pyridyl protons were observed

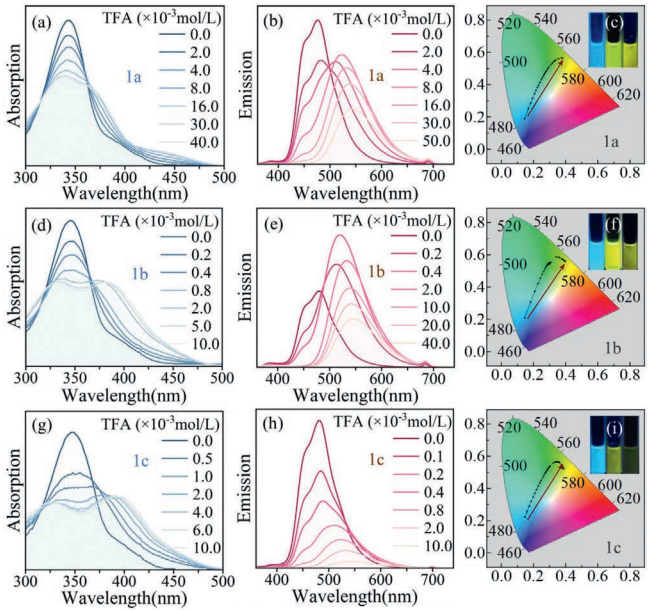


Fig. 5. UV–vis absorption spectra of (a) **1a**, (d) **1b**, and (g) **1c** in toluene at a concentration of 2×10^{-6} mol/L upon the addition of TFA. Emission spectra of (b) **1a**, (e) **1b**, and (h) **1c** in toluene at a concentration of 2×10^{-6} mol/L upon the addition of TFA ($\lambda_{exc} = 340$ nm). Chromaticity change in the CIE coordinate diagrams and insets for the photoluminescence images of (c) **1a**, (f) **1b**, and (i) **1c**.

(Figs. S2-S4 in Supporting information). The downfield shifts are consistent with the enhanced electron-withdrawing effect induced by protonation. The calculated $\log K_{1-4}{}^H$ (Table S8 in Supporting information) indicates that the ability for binding one proton follows the order of aza[10]CPP > diaza[10]CPP > tetraaza[10]CPP. When the molecule contains multiple pyridyl groups, increased number of bound protons would lead to weaker overall proton-binding ability, which was also validated by electrostatic potentials (Fig. S11 in Supporting information).

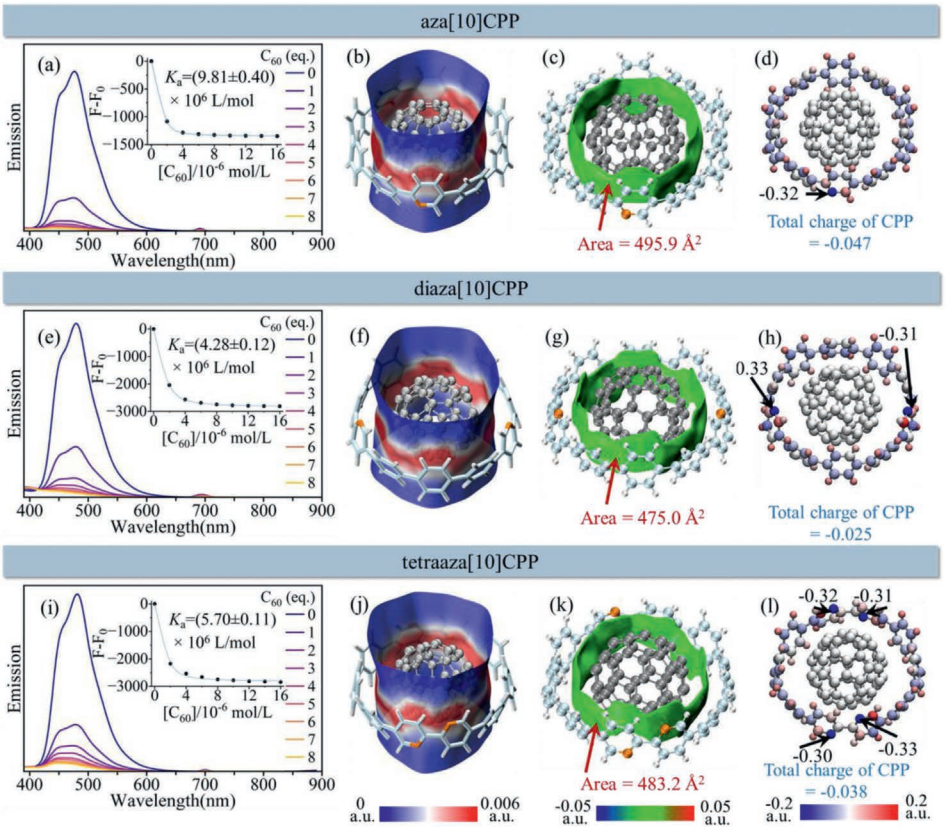


Fig. 6. Fluorescence quenching experiments and visualized weak intermolecular interaction analysis between N-doped nanohoops and C_{60}: Changes in fluorescence spectra (λ_{exc} = 345 nm) upon addition of C_{60} (0.0–1.6 × 10^{-5} mol/L) for (a) **1a**, (e) **1b**, and (i) **1c** in toluene with the concentration of 2.0 × 10^{-6} mol/L. Insets: Binding isotherms and nonlinear fitting according to a 1:1 model for **1a** (at 477 nm), **1b** (at 480 nm), and **1c** (at 481 nm). Hirshfeld surface maps to represent the interactions between C_{60} and (b) **1a**, (f) **1b**, and (j) **1c**. IGMH maps of C_{60} with (c) **1a**, (g) **1b**, and (k) **1c** with isovalue of 0.002 a.u. Colouring atoms according to atomic charges of (d) **1a**, (h) **1b**, and (l) **1c** using Multiwfn.

Considering the similar structures of these azananohoops as the parent nanohoop [10]CPP, which is of particular interest due to its ability to selectively encapsulate fullerene guests with high binding constants (K_a) [28], we next investigated the impact of N-doping on host-guest properties. The fluorescence titration experiments were carried out by adding fullerene guest (C_{60}) incrementally to the solution of CPP hosts, while the concentration of which was kept constant. The fluorescence of the CPP solution was completely quenched as the accumulation of the amount of C_{60}, and K_a was readily determined to be (9.81 ± 0.40) × 10^6L/mol for aza[10]CPP (**1a**), (4.28 ± 0.12) × 10^6L/mol for diaza[10]CPP (**1b**), and (5.70 ± 0.11) × 10^6L/mol for tetraaza[10]CPP (**1c**), respectively by fitting the binding isotherms to a 1:1 stoichiometric model (Figs. 6a, e and i).

It can be found that all three N-doped [10]CPPs exhibit higher affinity to C_{60} than the parent nanohoop [10]CPP. Besides, the binding constant of aza[10]CPP with single N-doping is higher than another two azananohoops. To better understand this result, we performed a comprehensive theoretical analysis of the interactions between the host and the guest species. First, the interaction energy (ΔE_{int}) between N-doped nanohoops and C_{60} was calculated, which turns out to be −48.05 (C_{60}⊂aza[10]CPP), −46.82 (C_{60}⊂diaza[10]CPP), and −46.93 (C_{60}⊂tetraaza[10]CPP) kcal/mol, respectively with consideration of basis set superposition error (BSSE) correction. These values are almost equivalent to a weak chemical bond energy, suggesting a very strong binding strength between the host and the guest species. Hirshfeld surface maps (Figs. 6b, f and j) visually present the existence of strong intermolecular forces between N-doped nanohoops and C_{60} (red region). The interaction energy was further decomposed to analyze the influence of individual factor on the interactions using sobEDAw method (Table 1) [68]. Among the attractive forces with different kinds, the dispersion effects (ΔE_{disp}) play a dominant role (accounting for approximately 68%). The large, circular, and flat isosurfaces of IGMH maps of the complexes represent a typical π-π stacking interaction (green region) (Figs. 6c, g and k). The experimental values (K_a) correlate well with both isosurface area and ΔE_{int}, indicating that the binding affinity of the N-doped nanohoops with C_{60} has a strong relationship with π-π conjugation effect. As discussed previously, aza[10]CPP, diaza[10]CPP, and tetraaza[10]CPP exhibit different degrees of deviation from an ideal cylindrical shape, which may affect the degree of in-plane π-orbital overlaps and the orientation of the fragments, thereby influencing the dispersion attraction (π-π stacking) between the host and the guest. Apart from dispersion effect, electrostatic effects (ΔE_{els}) also play a certain role (accounting for approximately 23%) in the host-guest complexation process. The electrostatic

Table 1
The interaction energy (ΔE_{int}) for the complexation between azananohoops and C_{60}. ΔE_{int} can be decomposed into four parts: electrostatic energy (ΔE_{els}), orbital interaction (ΔE_{orb}), dispersion correction (ΔE_{disp}) and exchange-repulsion (ΔE_{xrep}).

Energy (kcal/mol)	C_{60}⊂aza[10]CPP	C_{60}⊂diaza[10]CPP	C_{60}⊂tetraaza[10]CPP
ΔE_{els}	−31.66 (23%)	−31.46 (23%)	−32.77 (24%)
ΔE_{orb}	−11.92 (9%)	−11.88 (9%)	−12.21 (9%)
ΔE_{disp}	−91.97 (68%)	−90.66 (68%)	−92.57 (67%)
ΔE_{xrep}	87.5	87.18	90.62
ΔE_{int}	−48.05	−46.82	−46.93

potential and atomic charge distribution revealed that the electrostatic attraction also facilitates the combination, as the surface of C_{60} carries a weak positive charge and the benzene rings of the nanohoops exhibit a weak negative charge (Figs. 6d, h and l, and Fig. S12 in Supporting information). Inserted nitrogen atoms enhanced electronegativity which might be one of the reasons why the N-inserted nanorings exhibit stronger binding ability with C_{60} than the parent [10]CPP. The electrostatic interaction of diaza[10]CPP is the weakest among the three azananohoops, which might be due to the fact that its structure is more deviated from circularity.

In summary, we have developed a synthetic methodology that would allow to access single, or multi pyridyl, or 2,2′-bipyridyl embedded [10]CPPs in a size-selective manner. Due to the insertion of nitrogen atoms, the shape of aza[10]CPP (**1a**) deviates from a perfect circle less significantly, while diaza[10]CPP (**1b**) presents as an irregular circle, and tetraaza[10]CPP (**1c**) slightly takes an elliptical shape after geometry optimization. Multiple insertions of nitrogen atoms also reduce the torsion angles and strain energies. Although the absorption intensity demonstrates an incremental decrease upon the addition of acid for all three azananohoops as expected, **1b** and **1c** show two shoulder absorptions arising at shorter and longer wavelengths, which are different from that of previously reported azaCPPs. Bathochromic shifts in emissions with reduced intensity were also observed for all three azananohoops under acidic conditions, while **1b** experienced a dramatic enhancement at low acid concentrations. Finally, the impact of N-doping on host-guest properties was studied by fluorescence titration experiments and theoretical calculations. All three N-doped [10]CPPs exhibit higher affinity for C_{60} than the parent nanohoop [10]CPP, with the binding constant of aza[10]CPP (**1a**) being the highest among them. Analysis of the interactions between the host and the guest species reveals that the dispersion effect arising from π-π stacking plays a dominant role in the complexation, while electrostatic attraction also contributes. Furthermore, both effects will be affected by the minor structural variations in the nanoring structures.

CRediT authorship contribution statement

Tianlu Wu: Methodology, Investigation, Formal analysis, Data curation. **Jiaojiao Yang:** Validation, Methodology, Investigation. **Yaru Liu:** Investigation, Formal analysis. **Chen Wang:** Investigation. **Jiwen Zhang:** Validation. **Ren-Hui Zheng:** Software, Resources. **Huan Yu:** Resources. **Rui Liu:** Writing – original draft, Software, Resources, Methodology, Investigation, Formal analysis. **Dapeng Lu:** Writing – review & editing, Supervision, Resources, Project administration, Funding acquisition, Formal analysis, Data curation, Conceptualization.

Declaration of interest statement

The authors declare that they have no known competing financial interests or personal relationships that could have appeared to influence the work reported in this paper.

Acknowledgments

This work was financially supported by the National Natural Science Foundation of China (No. 21801004), Anhui Provincial Natural Science Foundation (No. 2008085QB86), University Natural Science Research Project of Anhui Province (Nos. 2024AH050709, 2024AH050675), and Peak Discipline Funding of the School of Pharmacy of Anhui Medicinal University (No. 2023xkjd23).

Supplementary materials

Supplementary material associated with this article can be found, in the online version, at doi:10.1016/j.cclet.2025.112199.

References

[1] M. Hasegawa, Y. Nojima, Y. Mazaki, ChemPhotoChem 5 (2021) 1042–1058.
[2] Y. Li, H. Kono, T. Maekawa, et al., Acc. Mater. Res. 2 (2021) 681–691.
[3] R. Zhang, D. An, J. Zhu, X. Lu, Y. Liu, Adv. Funct. Mater. 33 (2023) 2305249.
[4] M.A. Majewski, M. Stępień, Angew. Chem. Int. Ed. 58 (2019) 86–116.
[5] Y. Lv, J. Lin, K. Song, et al., Sci. Adv. 7 (2021) eabk3095.
[6] S.E. Lewis, Chem. Soc. Rev. 44 (2015) 2221–2304.
[7] Y. Tsuchido, R. Abe, T. Ide, K. Osakada, Angew. Chem. Int. Ed. 59 (2020) 22928–22932.
[8] J.P. Mora-Fuentes, M.D. Codesal, M. Reale, et al., Angew. Chem. Int. Ed. 62 (2023) e202301356.
[9] Z. Sun, H. Tang, L. Wang, D. Cao, Chem. Eur. J. 31 (2025) e202404217.
[10] N. Grabicki, K.T.D. Nguyen, S. Weidner, O. Dumele, Angew. Chem. Int. Ed. 60 (2021) 14909–14914.
[11] X. Wang, F. Jia, L.P. Yang, H. Zhou, W. Jiang, Chem. Soc. Rev. 49 (2020) 4176–4188.
[12] K.Y. Cheung, S.J. Gui, C.F. Deng, et al., Chem 5 (2019) 838–847.
[13] L. Li, S.M. Long, N.J. Selvaraj, et al., Org. Lett. 27 (2025) 6578–6582.
[14] W. Fan, T.M. Fukunaga, S. Wu, et al., Nat. Synth. 2 (2023) 880–887.
[15] K. Wei, J. Li, W. Zhang, et al., Chin. Chem. Lett. 35 (2024) 109055.
[16] X. Li, L. Liu, L. Jia, et al., Nat. Commun. 16 (2025) 467.
[17] S. Zhong, L. Zhu, S. Wu, Y. Li, M. Lin, Chin. Chem. Lett. 34 (2023) 108124.
[18] H. Deng, Z. Guo, Y. Wang, et al., Chem. Sci. 13 (2022) 14080–14089.
[19] S. Chen, C. Zhang, X. Dong, H.J. Zhang, J. Lin, Chin. Chem. Lett. 36 (2025) 110354.
[20] Y. Segawa, M. Kuwayama, Y. Hijikata, et al., Science 365 (2019) 272–276.
[21] J.H. May, J.M. Van Raden, R.L. Maust, L.N. Zakharov, R. Jasti, Nat. Chem. 15 (2023) 170–176.
[22] P. Della Sala, A. Capobianco, T. Caruso, et al., J. Org. Chem. 83 (2018) 220–227.
[23] P.C. Hall, H.W. Reid, I. Liashenko, et al., Small 20 (2024) 2400882.
[24] B. Zou, J.A. Li, Z. Zhai, et al., Eur. J. Org. Chem. 27 (2024) e202400135.
[25] Y. Hu, T. Li, T. Su, et al., Chem. Sci. 16 (2025) 13115–13121.
[26] J. Mun, J. Kang, Y. Zheng, et al., Adv. Mater. 31 (2019) e1903912.
[27] P. Seitz, M. Bhosale, L. Rzesny, et al., Angew. Chem. Int. Ed. 62 (2023) e202306184.
[28] T. Iwamoto, Y. Watanabe, T. Sadahiro, T. Haino, S. Yamago, Angew. Chem. Int. Ed. 50 (2011) 8342–8344.
[29] K. Lan, C. Cheng, Sci. Sin. Chim. 53 (2023) 2402–2419.
[30] M. Freiberger, M.B. Minameyer, I. Solymosi, et al., Chem. Eur. J. 29 (2023) e202203734.
[31] Y. Yang, M. Juríček, ChemPlusChem 87 (2022) e202100468.
[32] O.A. Stasyuk, A.A. Voityuk, A.J. Stasyuk, M. Solà, Acc. Chem. Res. 57 (2024) 37–46.
[33] A. Stergiou, J. Rio, J.H. Griwatz, et al., Angew. Chem. Int. Ed. 58 (2019) 17745–17750.
[34] Y. Zhou, G. Zhuang, P. Du, Chin. Chem. Lett. 35 (2024) 108593.
[35] X. Li, Y. Liu, Z. Du, et al., Chin. Chem. Lett. 36 (2025) 110249.
[36] K.L. Zhu, Z.A. Li, J. Liang, Y. He, H.Y. Gong, Chin. Chem. Lett. 37 (2026) 111629.
[37] P. Li, Y. Jia, P. Chen, Chem. Eur. J. 29 (2023) e202300300.
[38] X. Sun, J. Bai, X.Y. Wang, H.Y. Gong, Coord. Chem. Rev. 518 (2024) 216063.
[39] K. Ikemoto, S. Harada, S. Yang, T. Matsuno, H. Isobe, Angew. Chem. Int. Ed. 61 (2022) e202114305.
[40] M. Zhu, Q. Zhou, H. Cheng, et al., Angew. Chem. Int. Ed. 62 (2023) e202213470.
[41] M. Chen, K.S. Unikela, R. Ramalakshmi, et al., Angew. Chem. Int. Ed. 60 (2021) 1556–1560.
[42] J. Nogami, D. Hashizume, Y. Nagashima, et al., Nat. Synth. 2 (2023) 888–897.
[43] S. Qiu, Y. Zhao, L. Zhang, et al., CCS Chem. 5 (2023) 1763–1772.
[44] S.H. Röttger, P.A. Mader, H.F. von Köller, P.G. Jones, D.B. Werz, Org. Lett. 27 (2025) 4969–4973.
[45] Y. Wang, S. Huang, Z. Zhang, X. Yan, J. Org. Chem. 89 (2024) 681–686.
[46] H. Zhang, J. Lin, Chin. J. Org. Chem. 42 (2022) 3437.
[47] Y. Xu, M.Y. Leung, L. Yan, et al., J. Am. Chem. Soc. 146 (2024) 13226–13235.
[48] X.W. Chen, Q.S. Deng, B.H. Zheng, et al., J. Am. Chem. Soc. 146 (2024) 31665–31670.
[49] K. Matsui, Y. Segawa, K. Itami, Org. Lett. 14 (2012) 1888–1891.
[50] E.R. Darzi, E.S. Hirst, C.D. Weber, et al., ACS Cent. Sci. 1 (2015) 335–342.
[51] J.M. Van Raden, S. Louie, L.N. Zakharov, R. Jasti, J. Am. Chem. Soc. 139 (2017) 2936–2939.
[52] C. Brouillac, N. McIntosh, B. Heinrich, et al., Adv. Sci. 11 (2024) e2309115.
[53] T. Drennhaus, D. Imoto, E.S. Horst, et al., Nat. Commun. 16 (2025) 4643.
[54] J. Xie, X. Li, Z. Du, Y. Liu, K. Zhu, CCS Chem. 5 (2023) 958–970.
[55] L. Zhan, C. Dai, G. Zhang, et al., Angew. Chem. Int. Ed. 61 (2022) e202113334.
[56] F. Schwer, S. Zank, M. Freiberger, et al., Org. Mater. 4 (2022) 7–17.
[57] J.H. Chen, T.Y. Huang, S. Tong, M.X. Wang, J. Am. Chem. Soc. 147 (2025) 1595–1603.
[58] I. González-Veloso, J. Rodríguez-Otero, E.M. Cabaleiro-Lago, Struct. Chem. 30 (2018) 647–656.
[59] D. Wu, W. Cheng, X.T. Ban, J.L. Xia, Asian J. Org. Chem. 7 (2018) 2161–2181.

[60] J. Xia, J.W. Bacon, R. Jasti, Chem. Sci. 3 (2012) 3018–3021.
[61] V.K. Patel, E. Kayahara, S. Yamago, Chem. Eur. J. 21 (2015) 5742–5749.
[62] Y. Segawa, H. Omachi, K. Itami, Org. Lett. 12 (2010) 2262–2265.
[63] C.E. Colwell, T.W. Price, T. Stauch, R. Jasti, Chem. Sci. 11 (2020) 3923–3930.
[64] R. Franklin-Mergarejo, D.O. Alvarez, S. Tretiak, S. Fernandez-Alberti, Sci. Rep. 6 (2016) 31253.
[65] T. Lu, F. Chen, J. Comput. Chem. 33 (2012) 580–592.
[66] T. Lu, Section 3.21.8 of Multiwfn manual Version 3.8, 2024 (accessed 23/08) available at http://sobereva.com/multiwfn .
[67] D.A. Hines, E.R. Darzi, E.S. Hirst, R. Jasti, P.V. Kamat, J. Phys. Chem. A 119 (2015) 8083–8089.
[68] T. Lu, Q. Chen, J. Phys. Chem. A 127 (2023) 7023–7035.